Research paper

Keggin-Al$_{30}$: An intercalant for Keggin-Al$_{30}$ pillared montmorillonite

Ke Wen[a,b,1], Jingming Wei[a,b], Hongping He[a,b], Jianxi Zhu[a,b,*], Yunfei Xi[c,d,*]

[a] CAS Key Laboratory of Mineralogy and Metallogeny, Guangdong Provincial Key Laboratory of Mineral Physics and Materials, Guangzhou Institute of Geochemistry, Chinese Academy of Sciences, 511 Kehua Street, Guangzhou 510640, China
[b] University of Chinese Academy of Sciences, Beijing 100049, China
[c] School of Earth, Environmental and Biological Sciences, Queensland University of Technology, 2 George Street, Brisbane, Qld 4001, Australia
[d] Institute for Future Environments, Queensland University of Technology, 2 George Street, Brisbane, Qld 4001, Australia

ABSTRACT

Clay minerals intercalated with inorganic species, known as pillared interlayered clays, have received extensive attention in recent decades. In this work, by comparison with those of Keggin-Al$_{13}$, the formation processes of Keggin-Al$_{30}$ are discussed based on different hydrolysis reactions. X-ray diffraction (XRD), field-emission scanning electron microscope, and thermogravimetric analyses were applied to compare differences in crystal structure, morphology, and thermal stability between Keggin-Al$_{13}$ and Keggin-Al$_{30}$ (sulfates). High temperature and excess monomeric Al species are key factors controlling the transformation from ε-Keggin-Al$_{13}$ to δ-Keggin-Al$_{13}$ and finally to Keggin-Al$_{30}$. A decrease of the crystal symmetry from Keggin-Al$_{13}$ to Keggin-Al$_{30}$ was confirmed by shifts of reflections (and decreases of intensities) on XRD patterns. Keggin-Al$_{30}$ has a more compact structure, which leads to higher thermal stability. The distributions of functional groups and positive charges on the surface of Keggin-Al$_{30}$ result in a "lying flat" arrangement configuration in the interlayer region of montmorillonite. Exploring the behaviors of polycations as intercalants from their formation, transformation, and properties during the pillaring process may offer better understandings of the enhanced properties and wide applications of pillared interlayered clays.

1. Introduction

Pillared interlayered clays (PILC) with inorganic polycations have been attracting increasing research interests since the early 1970s, when the aluminum intercalated clay family was introduced for the first time (Canizares et al., 1999; Gil et al., 2010; Vicente et al., 2013). Numerous studies have demonstrated the widespread applications of PILC as adsorbents and supports, particularly environmentally friendly ones in many fields. For example, PILC can be used as adsorbents for heavy metals (Lenoble et al., 2002; Manohar et al., 2006; Georgescu et al., 2017) and organic matter (Danis et al., 1998; Zeng et al., 2013; Qin et al., 2014) in the purification of industrial wastewater and as supports or catalysts (Pinnavaia, 1983; Figueras, 1988) in chemical catalysis (Wu et al., 2016) or catalytic oxidation processes related to the decomposition of organic matter in water (Zuo and Zhou, 2006; Zuo et al., 2008; Liang et al., 2016) or volatile organic compounds in atmosphere (Zhu et al., 2007; Huang et al., 2010; Li et al., 2013). All of these applications arise from the excellent properties of PILC, such as large surface area, high thermal stability, strong surface acidity and

porous structure (Molinard et al., 1994; Hernando et al., 2002; Kloprogge et al., 2005).

Pillared solids are usually prepared by exchanging the charge-compensating cations (e.g., Ca^{2+}, Na^+) present in the interlayer regions of swelling clays with hydroxyl-metal polycations (Gil et al., 2000; Vicente et al., 2013). Under calcination, the inserted polycations yield rigid and thermally stable oxides, which retain the layered structure of clays without collapse. Bergaya (Vicente et al., 2013) composed a periodic table of elements for those metal ions studied as pillaring agents, including Al, Fe, Ti, Zr, Ge, V, Cr, Co, Ga, Ni, Cu, Zn, Y, Ta, and others. Many types of hydroxyl-metal polycations can serve as intercalants for pillaring clays. PILC with pillaring polycations of titanium (DurgaáPrasad, 1990; Valverde et al., 2003; Yuan et al., 2006), iron (Najjar et al., 2007; Catrinescu et al., 2012), chromium (Choudary et al., 1992; Li et al., 2009; De León et al., 2014), zirconium (Burch and Warburton, 1986; Bartley, 1988), and even mixed oxides (Molina et al., 2006; Catrinescu et al., 2011; Banković et al., 2012) have been emphasized because of their potential application as catalysts. Although the hydrolysis behavior of many metal cations is generally understood,

more intensive studies have been done on aluminum ions (Baes and Mesmer, 1976), which is the reason why Al-PILC was the first to be prepared and extensively documented.

Much fundamental work on PILC, particularly work with Al-pillared smectites has been carried out through the past decades, but numerous questions remain (Vicente et al., 2013). Challenges in the study of PILC were described in the book *Handbook of Clay Science* (Vicente et al., 2013). Two major challenges among these are to investigate and understand the real structure of intercalated species before and after heating in greater detail and to determine the types of bonds formed between clay mineral and pillars, which determine the stability of the pillared clay minerals. Thus, the real mechanism of the formation, transformation and properties of polycations during the pillaring process needs to be revealed. As various types of chemical reactions control the processes, many researchers have been pursuing answers by synthesizing different types of polycations based on the hydrolysis chemistry. Consequently, new types of polycations for pillaring clay minerals have always been in focus in the past few decades. However, to present, among the large family of polycations (hydroxy-metal polycations), only the structures of several kinds of hydroxyl-aluminum polycations have been confirmed.

With the great development of hydrolysis chemistry and analytical techniques in recent years, aluminum has been found capable of forming polynuclear species, even species with large particle sizes (Casey, 2006). For example, the two well-studied types of hydroxyl-aluminum polycations with a confirmed structure are Keggin-Al_{13} ($[Al_{13}O_4(OH)_{24}(H_2O)_{12}]^{7+}$) and Keggin-$Al_{30}$ ($[Al_{30}O_8(OH)_{56}(H_2O)_{24}]^{18+}$) (Casey et al., 2001). Keggin-Al_{30} can be formed easily by heating a Keggin-Al_{13} solution. μ_2-OH^a bridges in ε-Keggin-Al_{13} are the most labile hydroxo sites, as was confirmed by ^{17}O nuclear magnetic resonance (NMR) (Casey et al., 2000). The lability of these sites leads to the transformation of ε-Keggin-Al_{13} into δ-Keggin-Al_{14} when the former is capped with monomeric Al ions. δ-Keggin-Al_{14} polycations further dimerize and react with two other monomers to produce δ-Keggin-Al_{30}. The identification of these two polycations, Keggin-Al_{13} and Keggin-Al_{30}, provides effective methods for synthesizing PILC with excellent properties. Therefore, extensive studies focused on the preparation, characterization, properties and applications of Al-PILC (Keggin-Al_{13} pillared intercalated clay minerals) have been carried out during the past decades. However, little attention has been devoted to Keggin-Al_{30}, which has a higher net charge (more than 2.5 times the positive charge) and particle size (nearly twice large) than Keggin-Al_{13}. Once it becomes possible to insert Keggin-Al_{30} into interlayer regions of clay minerals (e.g., montmorillonite, Mt), materials with excellent properties (e.g., many more micro/mesopores, large amounts of strong surface acid sites, etc.) will be obtainable.

In the previous work, well-crystallized Keggin-Al_{30} polycations were successfully intercalated into the interlayer regions of Mt for the first time (Zhu et al., 2017). This novel material demonstrates higher specific surface area, more micropores, enhanced thermal stability, and more surface acid sites, particularly the weak acid sites and very strong acid sites, than conventional Keggin-Al_{13} pillared intercalated Mt (Al_{13}-PILMt) (Zhu et al., 2017; Zhu et al., 2018; Wen et al., 2019). However, the behavior of Keggin-Al_{30} during the formation of Al_{30}-PILMt remains unknown, and how it contributes to the excellent properties of Al_{30}-PILMt is unclear. Therefore, the present work mainly focuses on the formation, transformation, and properties of Keggin-Al_{30} during the processes of hydrolysis and pillaring as an intercalant into Mt, even under calcination conditions. It aims to build linkages among the properties and transitions of the polycations, the chemical surroundings of the Mt layers, and the chemical reactions during the intercalation and pillaring processes.

2. Experimental

2.1. Materials

Calcium-montmorillonite (Mt) was obtained from Inner Mongolia, China. The Mt had a very high purity of more than 95% and a small amount of quartz (as an impurity), which was identified by powder X-ray diffraction (XRD) measurement. The main chemical compositions (wt.%) of the Mt were investigated by X-ray fluorescence (XRF), and the results were as follows: SiO_2 59.28%, Al_2O_3 15.93%, Fe_2O_3 5.25%, MgO 4.72%, CaO 2.42%, Na_2O 0.65%, P_2O_5 0.31%, TiO_2 0.27%, K_2O 0.09%, and the ignition loss was 9.63%. The cation exchange capacity (CEC) of this Mt, determined by the adsorption quantity of $[Co(NH_3)_6]^{3+}$ (He et al., 2010; Zhu et al., 2014), was 110.5 cmol/100 kg (Wang et al., 2016). The raw Mt was used directly without further purification because the extremely small amount of impurity (quartz) had little effect on the results. Aluminum chloride ($AlCl_3 \cdot 6H_2O$), sodium sulfate (Na_2SO_4), sodium hydroxide (NaOH), and silver nitrate ($AgNO_3$) were purchased from the Guangzhou Chemical Reagent Factory. All chemicals were of analytical grade and used as received. Distilled water (18.2 MΩ) from an ultrapure water purifier was used in all experiments.

2.2. Synthesis of pillared products

Intercalating solutions of Keggin-Al_{13} (Al_{13}-Int) and Keggin-Al_{30} (Al_{30}-Int) were prepared using the same method reported in previous study (Zhu et al., 2017). Within a water bath at 60 °C and vigorous stirring, a solution of NaOH (0.6 M) was added dropwise at a rate of 1 mL/min into an $AlCl_3$ solution (1.0 M). The final ratio of $[OH^-]/[Al^{3+}]$ was 2.4 and the concentration of Al was 0.2 M. The polymeric hydroxyl-aluminum solutions with the main component of Keggin-Al_{13} polycations were obtained after continuous stirring for 12 h and aged at 60 °C for 24 h. The Al_{30}-Int was prepared in a similar manner as the Al_{13}-Int. A solution of NaOH (0.6 M) was added dropwise at a rate of 1 mL/min into a solution of $AlCl_3$ (1.0 M) under constant stirring in an oil bath at 95 °C, yielding a final molar ratio value of $[OH^-]/[Al^{3+}]$ of 2.4. The final concentration of Al in the mixture obtained was also 0.2 M. The resulting solution was stirred at 95 °C for another 12 h and aged at 95 °C for 1 day. Then, the Al_{30}-Int was obtained.

The intercalated Mt with Keggin-Al_{13} and Keggin-Al_{30}, respectively, was prepared by ion exchange reactions, with an Al/clay ratio of 4.0 mmol/g. Under vigorous stirring, Mt powder was dispersed into Al_{13}-Int at 60 °C and into Al_{30}-Int at 95 °C. The two dispersions were stirred continuously for 24 h and then aged for 24 h at 60 °C and 95 °C, respectively. After being cooled to the room temperature (25 °C), the resultant products were separated by filtration and washed with distilled water until the supernatant solution was free of chloride as indicated by $AgNO_3$ solution. The collected solid products were freeze-dried for 48 h and denoted as Al_{13}-IntMt and Al_{30}-IntMt, respectively. Pillared intercalated samples were obtained after calcination at high temperature under an air atmosphere. The calcined samples were denoted as Al_{13}-PILMt-*x* and Al_{30}-PILMt-*x*, respectively, where *x* denotes the calcination temperature.

2.3. Synthesis of crystalline polyhydroxy-aluminum sulfates

As reported in many studies (Allouche et al., 2000; Aouad et al., 2006; Sivaiah et al., 2010; Miri et al., 2011), polycations of Keggin-Al_{30} can be separated by crystallization to form crystals with the presence of SO_4^{2-}. A 0.5 M Na_2SO_4 solution was added to the previously prepared Al_{13}-Int and Al_{30}-Int under vigorous stirring, obtaining the $[SO_4^{2-}]/[Al^{3+}]$ ratio of 0.33, to synthesize the crystalline sulfates of Keggin-Al_{13} and Keggin-Al_{30}, respectively. The precipitates, which formed after 3 days, were filtered, washed with distilled water, and air-dried for 24 h at room temperature. They were denoted as Al_{13}-$(SO_4)_n$ and Al_{30}-$(SO_4)_n$, respectively.

2.4. Characterization methods

Powder X-ray diffraction (XRD) patterns were obtained using Ni-filtered Cu Kα radiation (λ = 0.154 nm) on a Bruker D8 Advance diffractometer, which was operated at 40 kV and 40 mA with a scan rate of 3°/min (2θ) between 3° and 60°. Basal spacings were determined from the 2θ values of the corresponding basal reflections.

Thermogravimetric (TG) analysis was conducted on a Netzsch STA 409 PC thermal analysis instrument. Samples (approximately 15–20 mg, finely ground) were heated from 30 to 1000 °C at a speed of 10 °C/min under a constant flow of high-purity N_2 (60 mL/min). Derivative thermogravimetric (DTG) curves were derived from the TG curves of the same sample.

The morphology of each crystalline polyaluminum sulfate sample was recorded by a ZEISS SUPRA 55 SAPPHIRE field-emission scanning electron microscope. The finely ground sample powder was stuck to a conductive silver adhesive on a glass slide and subsequently sprayed with a thin layer of conductive carbon to enhance the conductivity before observation.
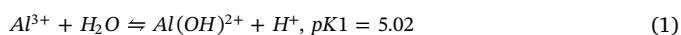
3. Results and discussions

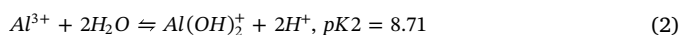### 3.1. Properties of pillared products

The properties of the Al_{30}-PILMt and Al_{13}-PILMt were reported in previous studies (Zhu et al., 2017; Zhu et al., 2018; Wen et al., 2019). Briefly, Al_{30}-IntMt shows a much larger d-spacing (1.95 nm) than Al_{13}-IntMt (1.86 nm), even after calcination at 300 °C (Al_{30}-PILMt, 1.86 nm; Al_{13}-PILMt, 1.65 nm). Much larger specific surface area and porosity were obtained by pillaring with Keggin-Al_{30} than with Keggin-Al_{13}. Al_{30}-PILMt shows a higher thermal stability than Al_{13}-PILMt. An abundance of micropores and mesopores was still retained in the Al_{30}-PILMt, and the layers of Mt did not collapse, even under the calcination temperature of 800 °C. The arrangement of Keggin-Al_{30} polycations in the interlayer region of Mt is also very different from that of Keggin-Al_{13}. Tracking the behaviors of Keggin-Al_{30} and Keggin-Al_{13} during the pillaring processes may provide an opportunity to determine how the polycation properties affect the characteristics of the pillared products.

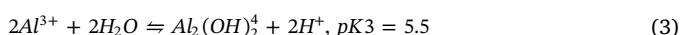### 3.2. Formation of Keggin-Al_{30} from Keggin-Al_{13}

Aluminum (Al) is the most abundant metal in the Earth's crust. It exhibits only the trivalent state in its compounds and solutions. With an ionic radius of 0.5 Å, Al^{3+} has a hydration number of 6 as $[Al(OH_2)_6]^{3+}$ in water. Like many other cations, Al^{3+} can be hydrolyzed extensively to form solutions of polynuclear hydroxide species which can be stable indefinitely but in fact are metastable with respect to the precipitation of the hydroxide [$Al(OH)_3$, gibbsite]. These reactions are commonly quite slow at room temperature, and can form different kinds of less stable large polymeric or colloidal species in solution. The reactions can be expressed as follows:
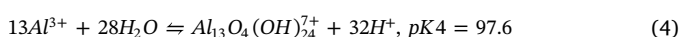
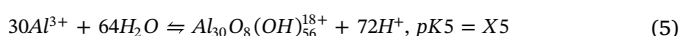$$Al^{3+} + H_2O \leftrightharpoons Al(OH)^{2+} + H^+, \; pK1 = 5.02 \tag{1}$$

(Frink and Peech, 1963);

$$Al^{3+} + 2H_2O \leftrightharpoons Al(OH)_2^+ + 2H^+, \; pK2 = 8.71 \tag{2}$$

(Parks, 1972);

$$2Al^{3+} + 2H_2O \leftrightharpoons Al_2(OH)_2^4 + 2H^+, \; pK3 = 5.5 \tag{3}$$

(Bottero et al., 1980);

$$13Al^{3+} + 28H_2O \leftrightharpoons Al_{13}O_4(OH)_{24}^{7+} + 32H^+, \; pK4 = 97.6 \tag{4}$$

(Sillen et al., 1964);

$$30Al^{3+} + 64H_2O \leftrightharpoons Al_{30}O_8(OH)_{56}^{18+} + 72H^+, \; pK5 = X5 \tag{5}$$

From Eq. (5) – 2 Eq. (4), we obtain the following:
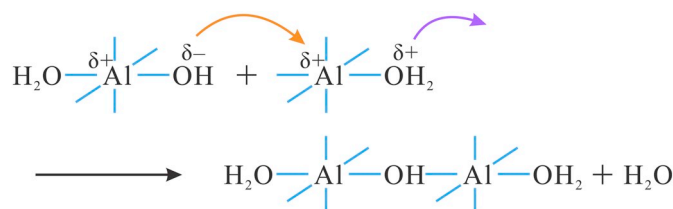
Fig. 1. Mechanism of olation reaction.

$$2Al_{13}O_4(OH)_{24}^{7+} + 4Al^{3+} + 8H_2O \leftrightharpoons Al_{30}O_8(OH)_{56}^{18+} + 8H^+, \; pK6 = X6 \tag{6.1}$$
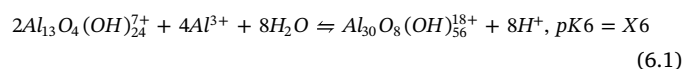
Here, $X_6 = X_5$–195.2
Interestingly, Eq. (6.1) – 4 Eq. (2) equals:

$$2Al_{13}O_4(OH)_{24}^{7+} + 4Al(OH)_2^+ \leftrightharpoons Al_{30}O_8(OH)_{56}^{18+}, \; pK7 = X7 \tag{6.2}$$
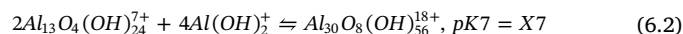
Here, $X_7 = X_6$–34.84 = X_5–230.04

The pH condition strongly affects the main polymeric species in the solution because of the production of H^+ in this process. Depending on the pH value of the solution, Al^{3+} can form $[Al(OH)_h(OH_2)_{6-h}]^{(3-h)+}$ aquaoxyhydroxo species in water. These species continuously produce polymeric species by undergoing condensation reactions (olation reaction, Fig. 1) with the elimination of water molecules and formation of hydroxo bridges (Baes and Mesmer, 1976). The rate of this process is usually very fast due to the high lability of water molecules (Jolivet et al., 2011). Several kinds of polymeric species, possibly with one dominant type, are likely to be present in the same solution under an equilibrium.

Under a water bath at 60 °C, large amounts of monomeric species form firstly because of their highest solubility. With dropwise addition of NaOH solution into the hot $AlCl_3$ solution, monomeric species (Fig. 2A(1)) start to aggregate and form dimeric (Fig. 2A(2)) and trimeric (Fig. 2A(3)) species via the olation reactions. To form the Keggin-Al_{13} polycation, one tetrahedral aluminum becomes surrounded by four trimeric species of octahedral aluminum (Fig. 2A(4)). Both the heating temperature and aging process control the formation of Keggin-Al_{13} under the certain ratio of OH/Al of 2.4. The final pH value of the Keggin-Al_{13} solution is 3.93.

Under suitable chemical conditions, two Keggin-Al_{13} can further transfer to a Keggin-Al_{30} through combination with four $Al(OH)_2^+$ ions (Eq. (6.2), Fig. 2B). When the solutions are heated to 95 °C under an oil bath, hydrolysis reactions of Al^{3+} occur, forming the larger polymeric Keggin-Al_{30} due to the higher energy obtained. The final pH value of the Keggin-Al_{30} solution is 4.21. The presence of excess monomeric species $[Al(OH_2)_6]^{3+}$ is another key factor for the formation of Keggin-Al_{30} (Allouche and Taulelle, 2003). Al monomers play two roles in this process: (1) Al monomers are the basic and necessary units for forming δ-Keggin-Al_{14} and connecting δ-Keggin-Al_{14} to form Keggin-Al_{30}, and (2) Al monomers can increase the ε-Keggin-Al_{13} dissolution rate and thus promote rearrangement and isomerization, which finally facilitate the formation of Keggin-Al_{30} (Phillips et al., 2003; Yang et al., 2010). Under the effect of Al^{3+} monomers (Fig. 2B(5)), ε-Keggin-Al_{13} is dissolved and rearranged to form δ-Keggin-Al_{13}. With the combination of basic units of Al^{3+} monomers, two δ-Keggin-Al_{13} together with four Al^{3+} monomers (Fig. 2B(6)) can form Keggin-Al_{30} (Fig. 2B).

3.3. Properties of Keggin-Al_{13} and Keggin-Al_{30}

3.3.1. X-ray diffraction of crystalline polyhydroxy-aluminum sulfates

The structural parameters of Keggin-Al_{13} were first reported in 1960 through investigation of the structures of its selenite and sulfate hydrates using XRD (Johansson, 1960; Johansson et al., 1960). The structure of Keggin-Al_{13} sulfate can be described as follows: cubic, space group F-43m, $a = b = c = 17.856$ Å, $\alpha = \beta = \gamma = 90°$ (Parker et al., 1997). Its structural formula is $Na[AlO_4Al_{12}(OH)_{24}(H_2O)_{12}]$

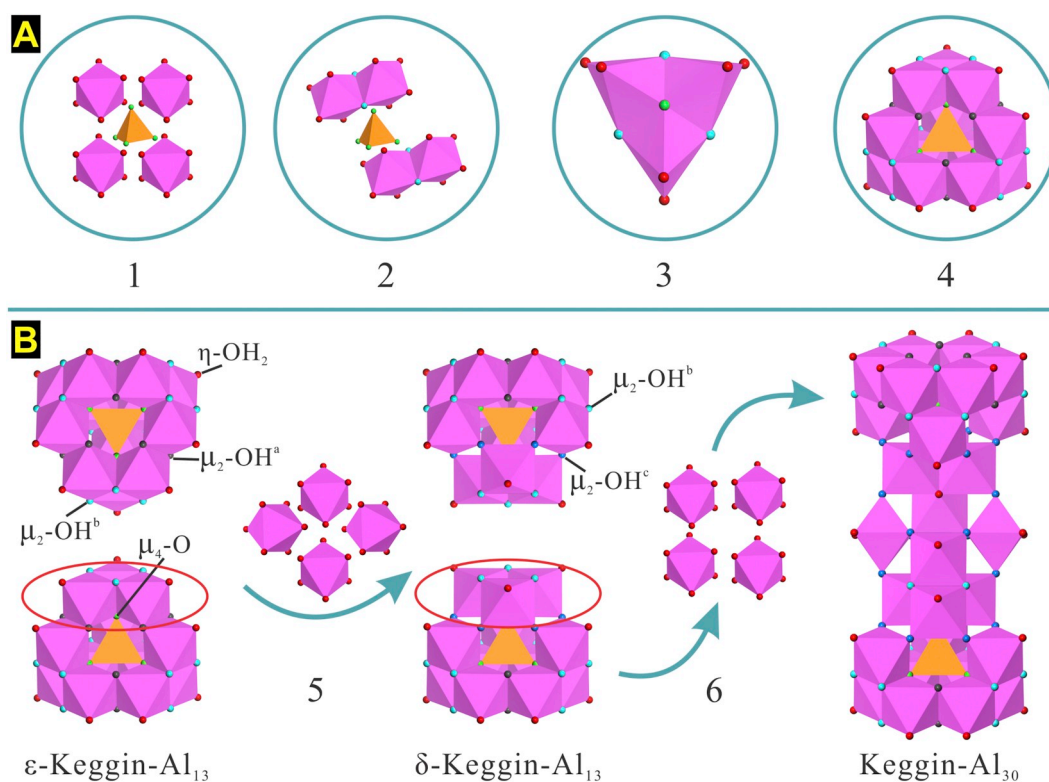**Fig. 2.** Schematic representation of the formation process for (A) Keggin-Al_{13} and (B) Keggin-Al_{30}. 1, monomeric Al; 2, dimeric Al; 3, trimeric Al; 4, Keggin-Al_{13}.

$(SO_4)_2 \cdot 10H_2O$. The structural parameters of Keggin-Al_{30} sulfate were obtained by X-ray crystal structure analysis in 2000 (Allouche et al., 2000; Rowsell and Nazar, 2000). The structure of Keggin-Al_{30} sulfate can be described as follows: monoclinic, space group $C2/c$, $a = 27.8238(10)$ Å, $b = 19.5008(7)$ Å, $c = 28.9659(11)$ Å, $\alpha = \gamma = 90°$, $\beta = 112.265(1)°$ (Rowsell and Nazar, 2000). Its structural formula is $[Al_2O_8Al_{28}(OH)_{56}(H_2O)_{26}](SO_4)_9 \cdot xH_2O$ ($x \approx 27$).

In the present study, structural parameters of the synthesized Keggin-Al_{13} and Keggin-Al_{30} sulfate hydrates were collected on a powder XRD instrument. Al_{13}-$(SO_4)_n$ and Al_{30}-$(SO_4)_n$ exhibited similar XRD patterns (Fig. 3). Strong reflections of (111), (222), and (333) occurred in both of their XRD patterns due to the typical Keggin-type structure. The XRD pattern of Al_{13}-$(SO_4)_n$ is in good accordance with the cubic structure of $NaAl_{13}(SO_4)_4 \cdot xH_2O$ (JCPDS No. 49-457) reported by Johansson in 1960 (Johansson, 1960). Notably, some variations can be observed in the pattern of Al_{30}-$(SO_4)_n$ when comparing with the pattern of Al_{13}-$(SO_4)_n$ (Fig. 3A). The intensities of the (111) and (222) reflections of Al_{30}-$(SO_4)_n$ are increased and those of (200) and (400) are decreased. Particularly, the (620) reflection even disappears in the XRD pattern of Al_{30}-$(SO_4)_n$. In addition, a left shift toward smaller 2θ and larger d-value occurs for the (111) reflection of Al_{30}-$(SO_4)_n$ (Fig. 3B). All of these variations of XRD pattern of Al_{30}-$(SO_4)_n$ result from the differences of its structure when compared with Al_{13}-$(SO_4)_n$. ε-Keggin-Al_{13} has a very high cubic crystalline symmetry (Fig. 2A(4)). When it transforms into δ-Keggin-Al_{13}, the degree of symmetry decreases slightly (Fig. 2B(5)). Through combination with the four monomers, two δ-Keggin-Al_{13} are connected to form one monoclinic Keggin-Al_{30} (Fig. 2B), with further decreases of crystal symmetry. Additionally, d values of the (111) group planes in both crystals can be obtained from the calculation of d-spaces based on their structural parameters using equations as follows:

Al_{13}-$(SO_4)_n$, cubic:

$$d_{(111)} = \frac{a}{\sqrt{h^2 + k^2 + l^2}} = \frac{17.856}{\sqrt{1 + 1 + 1}} \approx 10.31 \text{ Å}, \tag{7}$$

Al_{30}-$(SO_4)_n$, monoclinic:

$$\frac{1}{d^2} = \frac{1}{(\sin\beta)^2}\left(\frac{h^2}{a^2} + \frac{k^2(\sin\beta)^2}{b^2} + \frac{l^2}{c^2} - \frac{2hl\cos\beta}{ac}\right)$$
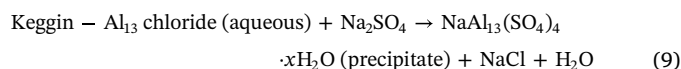
$$= \frac{1}{(\sin 112.265°)^2}$$

$$\left(\frac{1}{27.8238^2} + \frac{(\sin\beta 112.265°)^2}{19.5008^2} + \frac{1}{28.9659^2} - \frac{2\cos 112.265°}{27.8238 \times 28.9659}\right)$$

$$, d_{(111)} \approx 12.28 \text{ Å}, \tag{8}$$

The relationships of each (111) plane in the group planes can also be investigated by observing the atomic arrangements on the top views of the ($\bar{1}10$) planes (Fig. 4), which are perpendicular to those (111) planes in the crystal structures. Both methods provide the same explanation (decrease of degree of symmetry) for the slight shift of the (111) reflection in the pattern of Al_{30}-$(SO_4)_n$.

3.3.2. Morphology of crystalline polyhydroxy-aluminum sulfates

The crystalline polyhydroxy-aluminum sulfates of Keggin-Al_{13} and Keggin-Al_{30} exhibit different morphological characteristics (Fig. 5). With the addition of Na_2SO_4 solution into Al_{13}-Int for 3 days of crystallization, typical tetrahedral-shape crystals were obtained (Fig. 5B(1) and C(2 and 3)). These crystals correspond to the polyhydroxy-aluminum sulfates of Keggin-Al_{13}, Al_{13}-$(SO_4)_n$. The micrographs observed have good consistence with those in previous studies (Duong et al., 2005; Sivaiah et al., 2010; Miri et al., 2011) and are in agreement with the cubic structure of $NaAl_{13}(SO_4)_4 \cdot xH_2O$ (JCPDS No. 49-457) (Johansson, 1960). The simplified overall reaction scheme can be described as Eq. (9) (Aouad et al., 2006):

$$\text{Keggin} - Al_{13} \text{ chloride (aqueous)} + Na_2SO_4 \rightarrow NaAl_{13}(SO_4)_4$$

$$\cdot xH_2O \text{ (precipitate)} + NaCl + H_2O \tag{9}$$

The strip-shape (Fig. 5D(5)) and petal- or ovoid-shape (Fig. 5D(4)) crystals are sulfates of Keggin-Al_{30}, Al_{30}-$(SO_4)_n$. Crystallization time has the greatest effect on the final shape mostly (Chen et al., 2007).

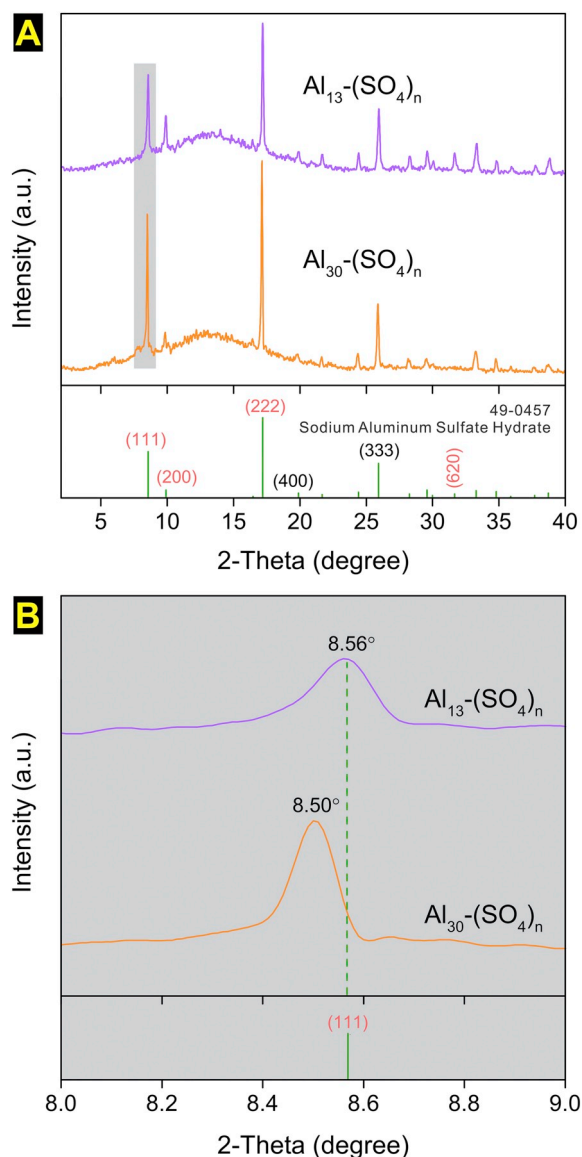**Fig. 3.** Powder X-ray diffraction patterns of Al_{13}-$(SO_4)_n$ and Al_{30}-$(SO_4)_n$, (B) is the enlarged view of the small region (shaded area) in (A).

3.3.3. Thermal analysis of polyhydroxy-aluminum sulfates

As shown in the TG-DTG curve of Keggin-Al_{13} sulfate, Al_{13}-$(SO_4)_n$ (Fig. 6A), three major mass loss stages, corresponding to the DTG peaks at 128 °C, 283 °C and 764 °C, respectively, are present in the TG curve. These stages arose from the removal of adsorbed and external water molecules (first stage, 18.3%), the dehydroxylation of the external six-coordinated Al of Keggin-Al_{13} (second stage, 21.6%), and the dehydroxylation of the internal surface of four-coordinated Al (third stage, 11.1%), respectively. Based on the approximate chemical formula of Al_{13}-$(SO_4)_n \cdot xH_2O$, the calculated total mass loss is approximately 47.6%, which is less than the actual experimental value of 51.0%. This difference was caused by the increased adsorbed water molecules on the surface of Al_{13}-$(SO_4)_n$ in the actual case. Similarly, three major mass loss stages, corresponding to the DTG peaks at 118 °C, 305 °C and 758 °C, respectively, occur in the TG curve of Keggin-Al_{30} sulfate, Al_{30}-$(SO_4)_n$ (Fig. 6B). They arose from the removal of adsorbed and external water molecules (first stage, 14.8%), the dehydroxylation of the external six-coordinated Al of Keggin-Al_{30} (second stage, 19.9%), and the dehydroxylation of the internal surface of four-coordinated Al (third stage, 13.0%), respectively. Calculated from the approximate chemical formula of Al_{30}-$(SO_4)_n \cdot xH_2O$, the total theoretical mass loss is approximately 43.6%, less than the actual experimental value of 47.8%. This difference was caused by the increased adsorbed water molecules on the surface of the Al_{30}-$(SO_4)_n$.

The TG-DTG curve of Al_{30}-$(SO_4)_n$ shows characteristics similar to those of Al_{13}-$(SO_4)_n$, suggesting that the removal of water molecules and the dehydroxylations happen at the comparable temperatures in both Al_{13}-$(SO_4)_n$ and Al_{30}-$(SO_4)_n$. The reasons for this observation can be discerned from structures of Keggin-Al_{13} and Keggin-Al_{30} (Fig. 7A and Fig. 7B). One Keggin-Al_{30} cation is composed of 2 units of Keggin-Al_{13} cation, with a linkage of four octahedral aluminum monomers (AlO_6, denoted as "1", "2", "3", and "4" in Fig. 7B, respectively). The hydroxyl group distribution on the surface of Keggin-Al_{30} is also similar to that of Keggin-Al_{13}, but with reduced structural symmetry overall. In a comparison to the third stage on the DTG curve of Al_{13}-$(SO_4)_n$ (Fig. 6A), a new small peak on the DTG curve of Al_{30}-$(SO_4)_n$ arises at 717 °C (Fig. 6B). It is speculated that this new peak at 717 °C can be ascribed to the dehydroxylation of quadridentate Al in Al_{30}-$(SO_4)_n$. Based on this assumption, according to their crystal chemical formula calculations, the third-stage mass loss of Al_{30}-$(SO_4)_n$ should include four more water molecules than that of Al_{13}-$(SO_4)_n$ (i.e., 2.0% greater mass loss in the third stage of the Al_{30}-$(SO_4)_n$ sample). Actually, an approximately 2.0% greater mass loss was observed in the experimental results of Al_{30}-$(SO_4)_n$. Thus, the speculation is highly consistent with the experimental results.

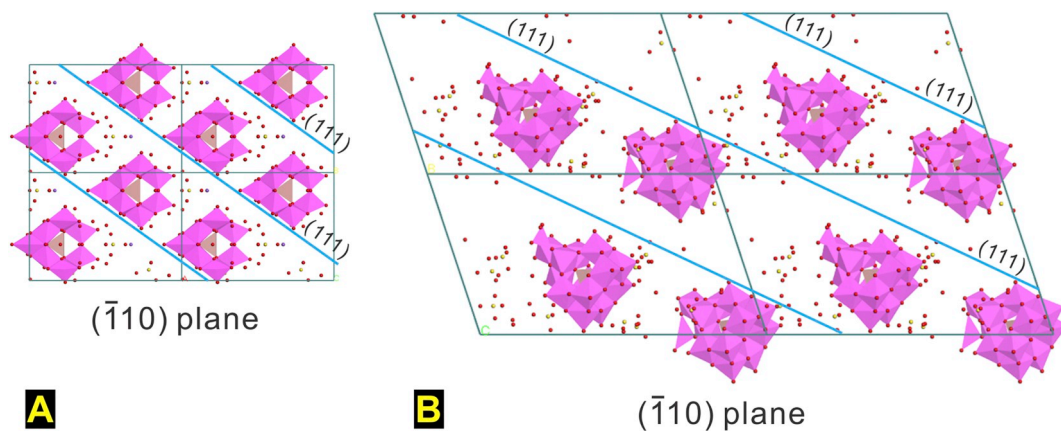**Fig. 4.** Polyhedral representation of the top views on ($\bar{1}$10) planes, (A) Al_{13}-$(SO_4)_n$ and (B) Al_{30}-$(SO_4)_n$; parallel lines represent the group planes of (111). Two δ-Keggin-Al_{14} polycations are bonded together with the combination of two monomeric species of Al^{3+}, together with a position shift in the (11$\bar{1}$) plane (B). Structural data references: Al_{13}-$(SO_4)_n$ (Johansson, 1960), Al_{30}-$(SO_4)_n$ (Allouche et al., 2000).
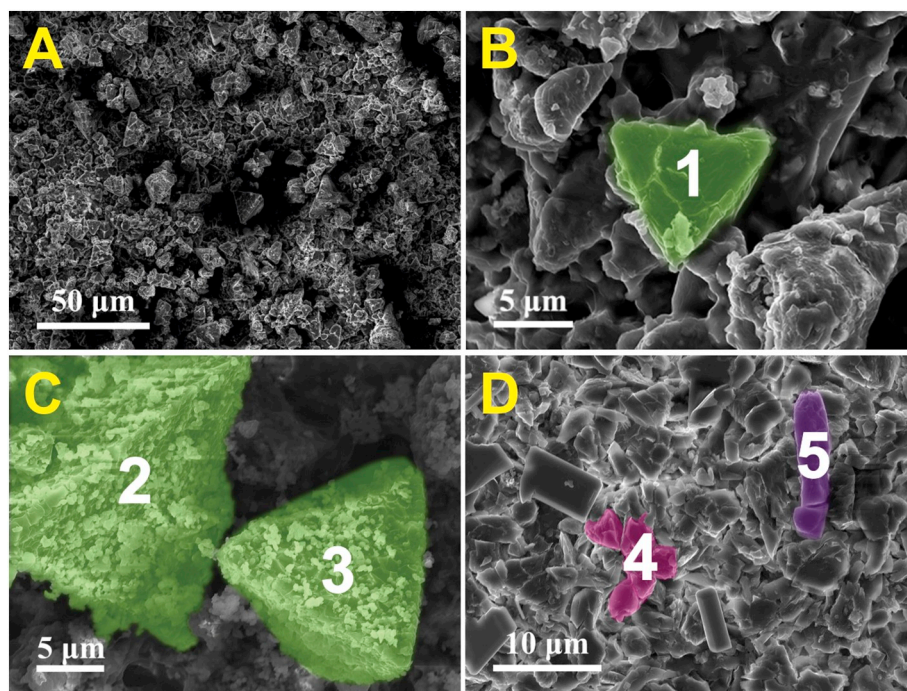
Fig. 5. Field emission scanning electronic (FE-SEM) micrographs of (A, B, C) Keggin-Al_{13} sulfates (1, 2, and 3) and (D) Keggin-Al_{30} sulfates with petal or ovoid shape (4) and strip-shape (5).
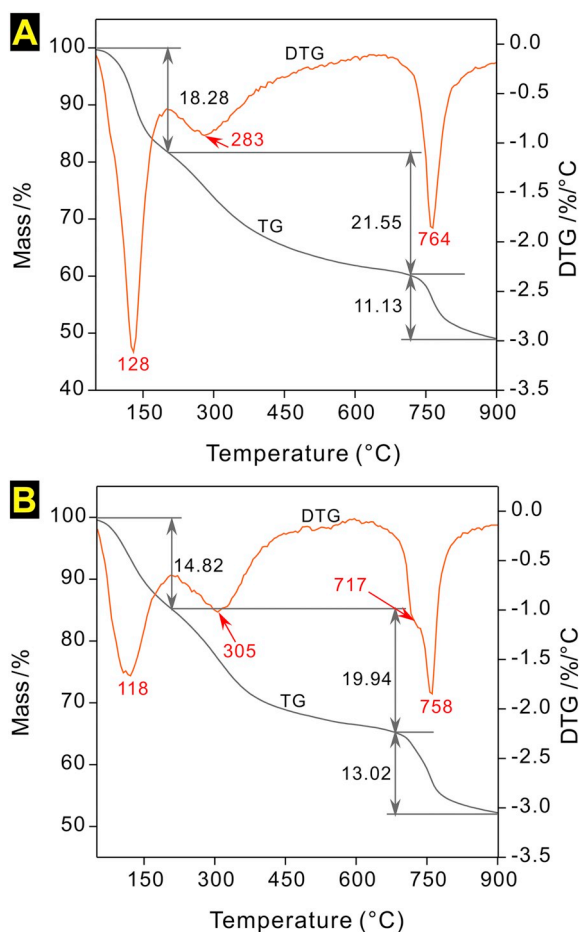

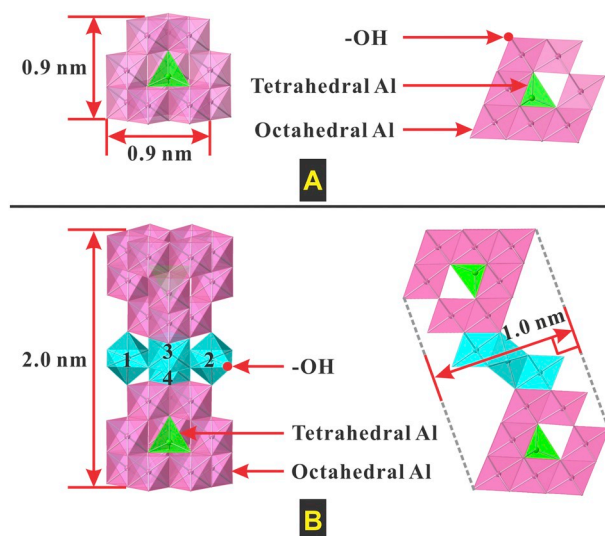**Fig. 6.** TG and DTG curves of (A) Al_{13}-$(SO_4)_n$ and (B) Al_{30}-$(SO_4)_n$.

Fig. 7. Schematic structural representation of (A) Keggin-Al_{13} and (B) Keggin-Al_{30}. Illustrations reproduced from Ref. (Zhu et al., 2017). Copyright (2017), with permission from Elsevier.

3.4. Behavior of polycations in the pillaring process

As reported in many studies (Gil et al., 2000; Kloprogge et al., 2005; Vicente et al., 2013), the procedure of pillaring consists of exchanging the exchangeable cations in the interlayer region of Mt (e.g., Na^+, Ca^{2+}, etc.) with polycations (e.g., Keggin-Al_{13} polycations). These polycations are then converted by heating into aluminum oxides, which act as pillars in the interlayer regions of Mt. In this study, the pillaring agents of Keggin-Al_{13} and Keggin-Al_{30} were synthesized first, followed by the intercalation process. This intercalation process is usually affected significantly by the characteristics of the polycations, such as the amount of positive charge, the type and arrangement of surface functional groups, and even the shape of the polycations.
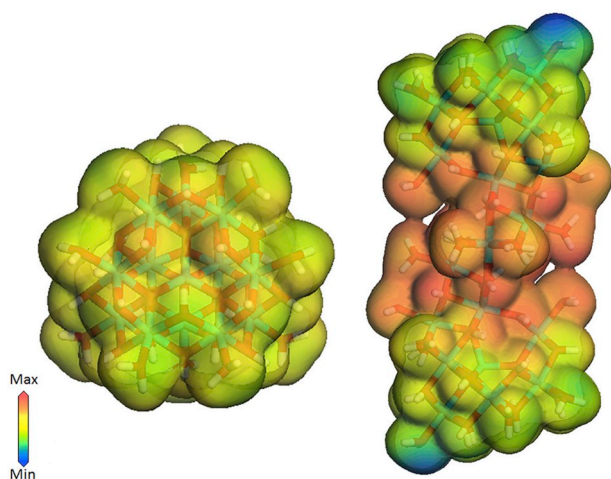
Fig. 8. Surface charge density of Keggin-Al$_{13}$ and Keggin-Al$_{30}$ (reproduced from Ref. Corum and Mason, 2016). The electrostatic potential is positive throughout, with higher positive values shown in red and lower positive values shown in blue. (For interpretation of the references to color in this figure legend, the reader can refer to the web version in Corum and Mason, 2016). Copyright (2016), with permission from Elsevier. (For interpretation of the references to color in this figure legend, the reader is referred to the web version of this article.)

By using the DFT calculations with sulfate and chloride as adsorption probes, the reactivities of Keggin-Al$_{13}$ and Keggin-Al$_{30}$ were determined as a function of particle topography (Corum and Mason, 2016). Keggin-Al$_{30}$, with its unique shape exhibits relatively strong adsorption in the molecular surroundings, as well as a wide range of reaction energies (Fig. 8). The reactivity on surfaces of polycations can affect the arrangement models in the interlayer region of Mt. As discussed in our previous study based on XRD results, chemical composition analysis, and calculation of structural formula, an arrangement model of Keggin-Al$_{30}$ "lying flat" in the interlayer region of Mt was proposed (Wen et al., 2019). The distribution of positive charges on the surface of Keggin-Al$_{30}$ (Fig. 8) influences its arrangement in Mt. Relatively larger amounts of positive charges and functional groups (η-OH$_2$, μ-OH^b and μ-OH^c, Fig. 2B) in the "waist" (surroundings of the four Al octahedral monomers that link the two Keggin-Al$_{13}$ polycations together) of Keggin-Al$_{30}$ facilitate interaction with the surfaces of Mt layers. Compared with Keggin-Al$_{13}$, each Keggin-Al$_{30}$ polycation can compensate more negative layer charge in Mt, because of the higher number of positive charges of Keggin-Al$_{30}$ (18) compared to Keggin-Al$_{13}$ (7). Surface positive charges on Keggin-Al$_{13}$ are distributed relatively evenly. Additionally, the cubic structure is more symmetrical and more similar to a sphere. When intercalating into the interlayer region of Mt, Keggin-Al$_{13}$ polycations can exist without any specific style due to the high degree of symmetry and the equally distributed charges on surfaces. These two types of polycations interact with the layers of Mt by electrostatic attractions.

During the calcination process to form pillared products, both Keggin-Al$_{13}$ and Keggin-Al$_{30}$ gradually loose water molecules with increasing temperature. The η-OH$_2$ type groups (Fig. 2B) on the surfaces will be lost first because of the relatively weak force of the Al-OH$_2$ bond. This step occurs simultaneously with the loss of adsorbed water molecules in the interlayer regions of Mt. The functional groups of μ-OH^a, μ-OH^b, and μ-OH^c on the surface (Fig. 2B) will are lost continuously via the dihydroxylation processes. Tetrahedral Al in the center of the polycation is protected and difficult to decompose. The two Al tetrahedrons in Keggin-Al$_{30}$ are different. The length of the Al—O bond in one of them is longer than the normal bond length. The η-OH$_2$ and μ-OH^c bonds in the "cap" of Keggin-Al$_{30}$ are shorter than those of Keggin-Al$_{13}$, and the O-Al-O bond angles (105.4–107.6°) in AlO$_4$

tetrahedra in Keggin-Al$_{30}$ are also smaller than those of Keggin-Al$_{13}$ (108.9–109.9°) (Yang et al., 2010). All these differences lead to a more compact structure of Keggin-Al$_{30}$, which results in the higher thermal stability than that of Keggin-Al$_{13}$ under high temperature. The transformation from ε-Keggin-Al$_{13}$ to δ-Keggin-Al$_{13}$ during the formation of Keggin-Al$_{30}$ causes this difference (Rowsell and Nazar, 2000; Yang et al., 2010). This is also the reason why a new peak occurred at around 70 ppm in the ^{27}Al NMR detection (Phillips et al., 2003). Finally, both Keggin-Al$_{13}$ and Keggin-Al$_{30}$ are converted into Al oxides under high temperature.

The existence of Keggin-Al$_{13}$ and Keggin-Al$_{30}$ polycations in the interlayer region of Mt can enhance the thermal stability of Mt, because of the protection provided by Al oxides as pillars. Due to the formation of pillars with high thermal stability in the interlayer region of Mt, layered structure and micro/mesoporous structures can be retained even at high temperatures. Particularly, Keggin-Al$_{30}$ has a great effect on protecting the layered structures of Mt at the calcination temperature of 800 °C because of the higher thermal stability of Keggin-Al$_{30}$ than Keggin-Al$_{13}$ (Casey et al., 2001; Zhu et al., 2018). Both the extremely high positive charge and the charge distribution on the surface of Keggin-Al$_{30}$ cause the specific "lying flat" arrangement in the interlayer region of Mt. The large size of Keggin-Al$_{30}$ and the specific distribution of Keggin-Al$_{30}$ polycations in the interlayer region of Mt results in the much larger specific surface area and porosity of Al$_{30}$-PILMt than Al$_{13}$-PILMt.

Conclusions

The properties of pillared products are dramatically affected by the characteristics of the intercalants, and tracking the behavior of polycations during the pillaring process can provide some insights. High temperature and excess monomeric Al species are key factors in the formation process of Keggin-Al$_{30}$. Keggin-Al$_{30}$ has a decreased crystal symmetry compared with Keggin-Al$_{13}$. The shorter η-OH$_2$ and μ-OH bond lengths and smaller O-Al-O bond angles in Keggin-Al$_{30}$ result in the more compact structure of Keggin-Al$_{30}$, which leads to its higher thermal stability compared with Keggin-Al$_{13}$. Concentrated positive charges on the "waist" of Keggin-Al$_{30}$ result in its "lying flat" arrangement in the interlayer region of Mt. This study revealed how the polycations of Keggin-Al$_{13}$ and Keggin-Al$_{30}$ form, key factors during the synthesis processes, and properties that dominate their behaviors as intercalants in the interlayer region of Mt. These findings could lead to better understandings of the effects of polycations on the enhanced properties and wide applications of PILC.

References

Allouche, L., Taulelle, F., 2003. Conversion of Al$_{13}$ Keggin ε into Al$_{30}$ a reaction controlled by aluminum monomers. Inorg. Chem. Commun. 6, 1167–1170.

Allouche, L., Gérardin, C., Loiseau, T., Férey, G., Taulelle, F., 2000. Al$_{30}$: a giant aluminum polycation. Angew. Chem. 112, 521–524.

Aouad, A., Pineau, A., Tchoubar, D., Bergaya, F., 2006. Al-pillared montmorillonite obtained in concentrated media. Effect of the anions (nitrate, sulfate and chloride) associated with the Al species. Clay Clay Miner. 54, 626–637.

Baes, C.F., Mesmer, R.E., 1976. Hydrolysis of Cations. Wiley.

Banković, P., Milutinović-Nikolić, A., Mojović, Z., Jović-Jovičić, N., Žunić, M., Dondur, V., Jovanović, D., 2012. Al, Fe-pillared clays in catalytic decolorization of aqueous tartrazine solutions. Appl. Clay Sci. 58, 73–78.

Bartley, G., 1988. Zirconium pillared clays. Catal. Today 2, 233–241.

Bottero, J.Y., Cases, J., Fiessinger, F., Poirier, J., 1980. Studies of hydrolyzed aluminum chloride solutions. 1. Nature of aluminum species and composition of aqueous

solutions. J. Phys. Chem. 84, 2933–2939.

Burch, R., Warburton, C., 1986. Zr-Containing pillared interlayer clays: II. Catalytic activity for the conversion of methanol into hydrocarbons. J. Catal. 97, 511–515.

Canizares, P., Valverde, J., Kou, M.S., Molina, C., 1999. Synthesis and characterization of PILCs with single and mixed oxide pillars prepared from two different bentonites. A comparative study. Microporous Mesoporous Mater. 29, 267–281.

Casey, W.H., 2006. Large aqueous aluminum hydroxide molecules. Chem. Rev. 106, 1–16.

Casey, W.H., Phillips, B.L., Karlsson, M., Nordin, S., Nordin, J.P., Sullivan, D.J., Neugebauer-Crawford, S., 2000. Rates and mechanisms of oxygen exchanges between sites in the $AlO_4Al_{12}(OH)_{24}(H_2O)_{12}^{7+}$(aq) complex and water: implications for mineral surface chemistry. Geochim. Cosmochim. Acta 64, 2951–2964.

Casey, W.H., Phillips, B.L., Furrer, G., 2001. Aqueous aluminum polynuclear complexes and nanoclusters: a review. Rev. Mineral. Geochem. 44, 167–190.

Catrinescu, C., Arsene, D., Teodosiu, C., 2011. Catalytic wet hydrogen peroxide oxidation of para-chlorophenol over Al/Fe pillared clays (AlFePILCs) prepared from different host clays. Appl. Catal. B Environ. 101, 451–460.

Catrinescu, C., Arsene, D., Apopei, P., Teodosiu, C., 2012. Degradation of 4-chlorophenol from wastewater through heterogeneous Fenton and photo-Fenton process, catalyzed by Al–Fe PILC. Appl. Clay Sci. 58, 96–101.

Chen, Z., Luan, Z., Fan, J., Zhang, Z., Peng, X., Fan, B., 2007. Effect of thermal treatment on the formation and transformation of Keggin Al_{13} and Al_{30} species in hydrolytic polymeric aluminum solutions. Colloids Surf. A Physicochem. Eng. Asp. 292, 110–118.

Choudary, B.M., Prasad, A.D., Bhuma, V., Swapna, V., 1992. Chromium-pillared clay as a catalyst for benzylic oxidation and oxidative deprotection of benzyl ethers and benzylamines: a simple and convenient procedure. J. Org. Chem. 57, 5841–5844.

Corum, K.W., Mason, S.E., 2016. Using density functional theory to study shape-reactivity relationships in Keggin Al-nanoclusters. Water Res. 102, 413–420.

Danis, T.G., Albanis, T.A., Petrakis, D.E., Pomonis, P.J., 1998. Removal of chlorinated phenols from aqueous solutions by adsorption on alumina pillared clays and mesoporous alumina aluminum phosphates. Water Res. 32, 295–302.

De León, M.A., De Los Santos, C., Latrónica, L., Cesio, A.M., Volzone, C., Castiglioni, J., Sergio, M., 2014. High catalytic activity at low temperature in oxidative dehydrogenation of propane with Cr–Al pillared clay. Chem. Eng. J. 241, 336–343.

Duong, L.V., Wood, B.J., Kloprogge, J.T., 2005. XPS study of basic aluminum sulphate and basic aluminium nitrate. Mater. Lett. 59, 1932–1936.

DurgaáPrasad, A., 1990. An improved asymmetric epoxidation of allyl alcohols using titanium-pillared montmorillonite as a heterogeneous catalyst. J. Chem. Soc. Chem. Commun. 1186–1187.

Figueras, F., 1988. Pillared clays as catalysts. Catal. Rev. Sci. Eng. 30, 457–499.

Frink, C., Peech, M., 1963. Hydrolysis of the aluminum ion in dilute aqueous solutions. Inorg. Chem. 2, 473–478.

Georgescu, A.-M., Nardou, F., Zichil, V., Nistor, I.D., 2017. Adsorption of lead (II) ions from aqueous solutions onto Cr-pillared clays. Appl. Clay Sci. 152, 44–50.

Gil, A., Gandia, L.M., Vicente, M.A., 2000. Recent advances in the synthesis and catalytic applications of pillared clays. Catal. Rev. 42, 145–212.

Gil, A., Korili, S.A., Trujillano, R., Vicente, M.A., 2010. Pillared Clays and Related Catalysts. Springer.

He, H., Ma, Y., Zhu, J., Yuan, P., Qing, Y., 2010. Organoclays prepared from montmorillonites with different cation exchange capacity and surfactant configuration. Appl. Clay Sci. 48, 67–72.

Hernando, M.J., Pesquera, C., Blanco, C., Gonza'lez, F., 2002. Increase in thermal stability of the texture in montmorillonites pillared with aluminum-cerium polyoxocations. Langmuir 4.

Huang, Q., Zuo, S., Zhou, R., 2010. Catalytic performance of pillared interlayered clays (PILCs) supported CrCe catalysts for deep oxidation of nitrogen-containing VOCs. Appl. Catal. B Environ. 95, 327–334.

Johansson, G., 1960. On the crystal structures of some basic aluminum salts. Acta Chem. Scand. 14, 771–773.

Johansson, G., Lundgren, G., Sillen, L., Soderquist, R., 1960. On the crystal structure of a basic aluminum sulfate and the corresponding selenate. Acta Chem. Scand. 14, 769–771.

Jolivet, J.-P., Chanéac, C., Chiche, D., Cassaignon, S., Durupthy, O., Hernandez, J., 2011. Basic concepts of the crystallization from aqueous solutions: the example of aluminum oxy (hydroxi) des and aluminosilicates. Compt. Rendus Geosci. 343, 113–122.

Kloprogge, J.T., Duong, L.V., Frost, R.L., 2005. A review of the synthesis and characterisation of pillared clays and related porous materials for cracking of vegetable oils to produce biofuels. Environ. Geol. 47, 967–981.

Lenoble, V., Bouras, O., Deluchat, V., Serpaud, B., Bollinger, J.-C., 2002. Arsenic adsorption onto pillared clays and iron oxides. J. Colloid Interface Sci. 255, 52–58.

Li, W., Wang, J., Gong, H., 2009. Catalytic combustion of VOCs on non-noble metal catalysts. Catal. Today 148, 81–87.

Li, D., Li, C., Suzuki, K., 2013. Catalytic oxidation of VOCs over Al-and Fe-pillared

montmorillonite. Appl. Clay Sci. 77, 56–60.

Liang, X., Qi, F., Liu, P., Wei, G., Su, X., Ma, L., He, H., Lin, X., Xi, Y., Zhu, J., 2016. Performance of Ti-pillared montmorillonite supported Fe catalysts for toluene oxidation: the effect of Fe on catalytic activity. Appl. Clay Sci. 132, 96–104.

Manohar, D., Noeline, B., Anirudhan, T., 2006. Adsorption performance of Al-pillared bentonite clay for the removal of cobalt (II) from aqueous phase. Appl. Clay Sci. 31, 194–206.

Miri, B., Bergaoui, L., Ghorbel, A., 2011. Synthesis and characterization of Al-pillared montmorillonite in presence of Mn (II). Appl. Clay Sci. 53, 691–695.

Molina, C., Casas, J., Zazo, J., Rodriguez, J., 2006. A comparison of Al-Fe and Zr-Fe pillared clays for catalytic wet peroxide oxidation. Chem. Eng. J. 118, 29–35.

Molinard, A., Clearfield, A., Zhu, H.Y., Vansant, E.F., 1994. Stability and porosity of aluminina-pillared clay in acid and basic solutions. Microporous Mater. 109–116.

Najjar, W., Azabou, S., Sayadi, S., Ghorbel, A., 2007. Catalytic wet peroxide photo-oxidation of phenolic olive oil mill wastewater contaminants: part I. Reactivity of tyrosol over (Al–Fe) PILC. Appl. Catal. B Environ. 74, 11–18.

Parker, W.O.N., Millini, R., Kiricsi, I., 1997. Metal substitution in Keggin-type tridecameric aluminum − oxo − hydroxy clusters. Inorg. Chem. 36, 571–575.

Parks, G.A., 1972. Free energies of formation and aqueous solubilities of aluminum hydroxides and oxide hydroxides at 25 C. Am. Mineral. 57, 1163–1189.

Phillips, B.L., Lee, A., Casey, W.H., 2003. Rates of oxygen exchange between the $Al_2O_8Al_{28}(OH)_{56}(H_2O)_{26}^{18+}$ (aq) (Al_{30}) molecule and aqueous solution. Geochim. Cosmochim. Acta 67, 2725–2733.

Pinnavaia, T.J., 1983. Intercalated clay catalysts. Science 220, 365–371.

Qin, Z., Yuan, P., Yang, S., Liu, D., He, H., Zhu, J., 2014. Silylation of Al_{13}-intercalated montmorillonite with trimethylchlorosilane and their adsorption for Orange II. Appl. Clay Sci. 99, 229–236.

Rowsell, J., Nazar, L.F., 2000. Speciation and thermal transformation in alumina sols: structures of the polyhydroxyoxoaluminum cluster $[Al_{30}O_8(OH)_{56}(H_2O)_{26}]^{18+}$ and its δ-Keggin moieté. J. Am. Chem. Soc. 122, 3777–3778.

Sillen, L.G., Martell, A.E., Bjerrum, J., 1964. Stability Constants of Metal-Ion Complexes. Chemical Society.

Sivaiah, M., Petit, S., Brendlé, J., Patrier, P., 2010. Rapid synthesis of aluminium polycations by microwave assisted hydrolysis of aluminium via decomposition of urea and preparation of Al-pillared montmorillonite. Appl. Clay Sci. 48, 138–145.

Valverde, J., De Lucas, A., Sanchez, P., Dorado, F., Romero, A., 2003. Cation exchanged and impregnated Ti-pillared clays for selective catalytic reduction of NO x by propylene. Appl. Catal. B Environ. 43, 43–56.

Vicente, M.A., Gil, A., Bergaya, F., 2013. Pillared clays and clay minerals. In: Bergaya, F., Lagaly, G. (Eds.), Developments in Clay Science, Second ed. Elsevier, pp. 523–557.

Wang, Y., Zhang, P., Wen, K., Su, X., Zhu, J., He, H., 2016. A new insight into the compositional and structural control of porous clay heterostructures from the perspective of NMR and TEM. Microporous Mesoporous Mater. 224, 285–293.

Wen, K., Zhu, J., Chen, H., Ma, L., Liu, H., zhu, R., Xi, Y., He, H., 2019. Arrangement models of Keggin-Al_{13} and Keggin-Al_{30} in the interlayer of pillared montmorillonite and the impacts of pillaring on surface acidity: a comparative study on catalytic oxidation of toluene. Langmuir 35, 382–390.

Wu, X., Xia, X., Liu, R., Chen, Y., 2016. Hydroxyalkylation of phenol to bisphenol F over Al-pillared clay. RSC Adv. 6, 34625–34632.

Yang, W., Qian, Z., Lu, B., Zhang, J., Bi, S., 2010. Density functional theory study and kinetic analysis of the formation mechanism of $Al_{30}O_8(OH)_{56}(H_2O)_{26}^{18+}$ (Al_{30}) in aqueous solution. Geochim. Cosmochim. Acta 74, 1220–1229.

Yuan, P., Yin, X., He, H., Yang, D., Wang, L., Zhu, J., 2006. Investigation on the delaminated-pillared structure of TiO_2-PILC synthesized by $TiCl_4$ hydrolysis method. Microporous Mesoporous Mater. 93, 240–247.

Zeng, L., Wang, S., Peng, X., Geng, J., Chen, C., Li, M., 2013. Al–Fe PILC preparation, characterization and its potential adsorption capacity for aflatoxin B1. Appl. Clay Sci. 83, 231–237.

Zhu, L., Tian, S., Zhu, J., Shi, Y., 2007. Silylated pillared clay (SPILC): a novel bentonitebased inorgano-organo composite sorbent synthesized by integration of pillaring and silylation. J. Colloid Interface Sci. 315, 191–199.

Zhu, R., Zhao, J., Ge, F., Zhu, L., Zhu, J., Tao, Q., He, H., 2014. Restricting layer collapse enhances the adsorption capacity of reduced-charge organoclays. Appl. Clay Sci. 88, 73–77.

Zhu, J., Wen, K., Zhang, P., Wang, Y., Ma, L., Xi, Y., Zhu, R., Liu, H., He, H., 2017. Keggin-Al_{30} pillared montmorillonite. Microporous Mesoporous Mater. 242, 256–263.

Zhu, J., Wen, K., Wang, Y., Ma, L., Su, X., Zhu, R., Xi, Y., He, H., 2018. Superior thermal stability of Keggin-Al_{30} pillared montmorillonite: a comparative study with Keggin-Al_{13} pillared montmorillonite. Microporous Mesoporous Mater. 265, 104–111.

Zuo, S., Zhou, R., 2006. Al-pillared clays supported rare earths and palladium catalysts for deep oxidation of low concentration of benzene. Appl. Surf. Sci. 253, 2508–2514.

Zuo, S., Huang, Q., Zhou, R., 2008. Al/Ce pillared clays with high surface area and large pore: synthesis, characterization and supported palladium catalysts for deep oxidation of benzene. Catal. Today 139, 88–93.